

Electromagnetic and microwave absorption properties of the core–shell structured C@BaMg_{0.2}Co_{0.8}TiFe₁₀O₁₉ nanoparticles

Jing Chen^{1,2} · Meiling Wang^{1,2} · Pingyuan Meng³ · Guangliang Xu²

Received: 25 July 2016 / Accepted: 1 October 2016 / Published online: 17 October 2016
© Springer Science+Business Media New York 2016

Abstract BaMg_{0.2}Co_{0.8}TiFe₁₀O₁₉ (BMCTF) hexaferrite was synthesized via sol–gel combustion reaction method, and the magnetic-dielectric heterostructured nanoparticles C@BMCTF was prepared by a combination of hydrothermal carbonization and carbothermal reduction processes (BMCTF as the core and carbon as the shell). From XRD, RAMAN, FE-SEM and HRTEM, the core–shell structure of C@BMCTF was confirmed and the average grain size of the particles was around 100–300 nm. Based on the static magnetic measurement, the coercivity (H_c) was increased and the saturation magnetization (M_s) was decreased with the coating of carbon. Moreover, the maximum reflection loss (RL) could reach -45.2 dB with a matching thickness of 1.8 mm from the electromagnetic parameters measured by vector network analyzer, and also the bandwidth of $RL \leq -10$ dB could cover the whole Ku band, which indicated the excellent absorbing properties of C@BMCTF.

1 Introduction

With the growing use of digital systems and microwave telecommunication systems, the electromagnetic (EM) absorbing materials which protect people from the electromagnetic wave have become a vital necessity [1, 2]. A microwave absorber absorbs electromagnetic energy when the impedance of free space is matched with the input characteristic impedance of an absorber, and then dissipates it as heat via both dielectric loss and magnetic loss [3].

The dielectric loss is caused by dielectric material and the magnetic loss is due to the magnetic component. In previous work, we have explained the necessity of effective matching of both the dielectric and magnetic component for good microwave absorption [4]. Numerous other reports are also available on this particular topic, where various dielectric materials and magnetic materials are combined to fulfill the aim of the effective microwave absorption. Han et al. [5] have showed the doping effect of MWCNT on the microwave absorption property of NiCoZn-spinel ferrite/MWCNT/wax hybrid composites. Zhang et al. [6] also have reported the maximum reflection loss (RL) value of -24.4 dB for Co_{0.5}Ni_{0.5}Fe₂O₄/carbon nanotubes/polyimide nanocomposites. With various types of microwave absorbing materials investigated, we come to the conclusion that the ferrite materials have a wide range of applications due to its strong magnetic loss [7–9]. Especially, M-type barium ferrite can be used in the whole GHz region because of its high resonance frequency (about 47.6 GHz), high resistivity, good chemical stability and low cost [10–13]. Du et al. [14] have confirmed that the magnetic resonance frequency can move to X band (8–12.4 GHz) by substituting cobalt ions (Co²⁺) and titanium ions (Ti⁴⁺) for Fe³⁺ in BaM. Wang et al. [7] have reported that the resonance frequency can be shifted to Ku

✉ Guangliang Xu
xuguangliang@swust.edu.cn

¹ State Key Laboratory Cultivation Base for Nonmetal Composites and Functional Materials, Southwest University of Science and Technology, Mianyang 621010, People's Republic of China

² School of Materials Science and Engineering, Southwest University of Science and Technology, Mianyang 621010, People's Republic of China

³ Huzhou Innovation Center of Advanced Materials, Shanghai Institute of Ceramics Chinese Academy of Sciences, Huzhou 215100, People's Republic of China

band (12.4–18) GHz in BaM when Fe^{3+} are partially substituted by metal ions Mn^{2+} and Ti^{4+} . Therefore, M-type barium ferrite composites are promising candidates for EM absorbing materials in the GHz range. However, the M-type barium ferrite has the magnetic loss as the main losses [10, 15], some shortcomings such as narrow band EM absorption and limitation of big density hinder for its wide application as an efficient EM absorber. Fortunately, carbon, as a light-weight dielectric material, can create interesting core–shell heterostructured nanoparticles with lower densities compared to other dielectric materials [16]. In order to improve the dielectric loss, the carbon has been doped in the ferrites. Jazirehpour et al. [17] have reported the maximum reflection loss (*RL*) value of -60 dB at 8.2 GHz for $\text{Fe}_3\text{O}_4@\text{C}$ nanocomposites with the thickness of about 2.6 mm. Therefore, the composite which contains dielectric and magnetic component should be developed, as the composite containing dielectric and magnetic component is likely to show the excellent microwave absorbing characteristics [18].

In the present work, we have prepared a hexagonal magnetoplumbite type ferrite $\text{BaMg}_{0.2}\text{Co}_{0.8}\text{TiFe}_{10}\text{O}_{19}$ (BMCTF) through a conventional sol–gel combustion technique and further used in the preparation of an effective core–shell structured microwave absorber through a combination of hydrothermal carbonization (HTC) carbon coating. A proper match has been provided between dielectric and magnetic properties through controlling the carbothermal reduction process.

2 Materials and methods

2.1 Preparation of BMCTF powders

Sample of hexagonal magnetoplumbite type ferrite BMCTF was synthesized using a conventional sol–gel combustion technique. The sample was synthesized from stoichiometric mixtures of analytical grade $\text{Mg}(\text{NO}_3)_2 \cdot 6\text{H}_2\text{O}$, $\text{Fe}(\text{NO}_3)_3 \cdot 9\text{H}_2\text{O}$, $\text{Ba}(\text{NO}_3)_2$, $\text{Ti}(\text{OC}_4\text{H}_9)_4$, $\text{Co}(\text{NO}_3)_2 \cdot 6\text{H}_2\text{O}$ and citric acid (AR, Sigma-Aldrich). In the solution preparation, the solution was stirred vigorously for 15 min in a magnetic stirrer to make it homogeneous. After complete dissolving, the solution of citric acid was added into the mixture, and then ammonia solution (AR, Sigma-Aldrich) was added dropwise with vigorous stirring until the value of PH was 7. Subsequently, the neutralized solution was heated with magnetic stirring to have the dried gel. If it continues to be heated, the dried gel would burn up in a self-propagating combustion manner, and some powders could be obtained. Finally, these powders were preheated with a heating rate of 5 °C/min at 450 °C for 4 h, and then calcined in air at 1100 °C for 4 h with a heating

rate of 5 °C/min to 650 °C and then 3 °C/min to the final elevated temperature in a furnace.

2.2 Surface treatment of BMCTF

To achieve the coating of glucose on BMCTF particles, the surface of BMCTF particles was modified in such a way that BMCTF became able to bind the glucose effectively on its surface. First, we dispersed the BMCTF particles in H_2O and then employed the sonication of the solution for 20 min in presence of polyacrylic acid (PAA). As the BMCTF particle had the tendency to aggregate, due to the magneto dipole interaction among the magnetic particles. PAA assisted to break that aggregation and to make a good dispersion of BMCTF particles. After that, the dispersed solution was treated by NaOH solution (0.2 M, 20 mL) in a mechanical stirrer for 15 min and the obtained product was washed with distilled water and ethanol several times. At last, the samples were dried in an oven at 55 °C.

2.3 Preparation of C@BMCTF

The hydroxyl modified surface of BMCTF particles was now ready to react efficiently with glucose, which was twice as much in weight ratio. At first, glucose and modified BMCTF nanocomposites were introduced into the distilled water and kept for 30 min in an ultrasonic bath after adding some PAA in it. Then, it was poured in the autoclave and kept for 6 h at 170 °C to carbonize the dissolved glucose under hydrothermal conditions, and the glucose might add to the hydroxyl modified BMCTF surface by forming H-bonds. After cooling the autoclave to room temperature, the resulting product was washed with distilled water and ethanol 3 times before dried. Finally, the product resulting from this process was annealed in a tube furnace under Ar flow at 600 °C for 50 min, as reduced samples were cooled to room temperature and then the gas flow was disconnected and the tube plug was removed.

2.4 Preparation of C@BMCTF composites

Firstly, the sample of C@BMCTF was dispersed in paraffin homogeneously with a sample-to-paraffin mass ratio of 85:15 and dissolved in xylene. Then, ultrasonicate for 20 min and keep it in the oven at 55 °C to remove the solvent completely. Finally, the mixture was pressed into a toroidal shape with an inner diameter of 3.00 mm and an outer diameter of 7.00 mm and thickness of about 2.0 mm.

2.5 Measurement of properties

The phase composition of samples were carried out by powder X-ray diffraction equipment (XRD, X'Pert PRO,

PANalytical, the Netherland), with Cu K α radiation ($k = 1.540598 \text{ \AA}$, 35 kV and 25 mA) in the range of 20–70° and a scan rate of 6 °/min. The components were ascertained by comparing the diffraction patterns with Joint Committee on Powder Diffraction Standards (JCPDS) cards, respectively. The size-distribution and morphology were characterized by the field emission scanning electron microscopy (FE-SEM, Ultra 55, ZEISS, Germany) and the high-resolution transmission electron microscope (HR-TEM, LIBRA 200FE, ZEISS, Germany). Raman spectroscopy was done with a Laser Raman Spectrometer (Renishaw, Britain) at room temperature. Static magnetic measurement was carried out on a vibrating sample magnetometer (VSM, BKT-4500Z, China) with a maximum magnetic field of 6 kOe. The scattering parameters were recorded on a vector network analyzer (Agilent Technologies, E8363A, USA) by using the coaxial measurements in the range of 0.5–18 GHz. The relative complex permittivity ($\epsilon_r = \epsilon' - j\epsilon''$) and permeability ($\mu_r = \mu' - j\mu''$) were extracted from the measured scattering parameters. The reflection loss was calculated by using the complex permittivity and permeability.

3 Results and discussions

As shown in Fig. 1, the detailed microstructures of the prepared materials were characterized by FE-SEM and HR-TEM. Figure 1a and b represented the SEM and TEM images of simple BMCTF, respectively, which suggested the formation of BMCTF particles with different sizes, and the most populated grain size range was 100–300 nm. Nevertheless, they displayed the irregular morphology except some bigger crystals, which had a significant hexagonal-shape. To show the coating of C on BMCTF, we

produced Fig. 1c and d. As can be seen in Fig. 1d, the HR-TEM image shown that the nanoparticles contained some dark shades, which was covered by light coloured frames, with a thickness of about 5 nm, in relation to sample BMCTF (Fig. 1b). We assumed that the dark coloured shades were due to the BMCTF particles, whereas, the light coloured frames were due to the formation of C on BMCTF. This difference in colour could be explained by considering the efficiency of electron penetration ability of BMCTF and C [19]. Moreover, although the content of C in the carbonized sample unable to confirm exactly through our testing instrument right now, it was evident that within a certain level, the thickness of the shell could be tuned with glucose amount.

Figure 2 showed the Raman analysis of C@BMCTF after the heat treatment under Ar atmosphere at 600 °C to confirm the presence of a carbon coating on the BMCTF particles. As seen in Fig. 2, two strong absorption peaks emerged at 1348 cm^{-1} (D band) and 1573 cm^{-1} (G band), and the other peaks were the characteristic peak of BMCTF. This observation was quite similar with the observation of Jazirehpour et al. [17]. The D band was indicative of the structural defects and disorders, while the G band was related to the C–C vibration of the carbon material with sp^2 orbital structure [20]. The intensity ratio of D and G peaks could be a criterion for assess the crystallinity of carbon materials. By considering I_D/I_G ($I_D/I_G = 1.078$) of the Raman spectrum curve, it could be found that the coated carbon on BMCTF was almost amorphous [21].

The X-ray diffraction pattern (a) in Fig. 3 showed that sample BMCTF, which was the precursor for C@BMCTF, had a single hexagonal magnetoplumbite phase (JCPDS Card No. 051-1879). Pattern (b) shown that all the diffraction peaks were in good agreements with those of

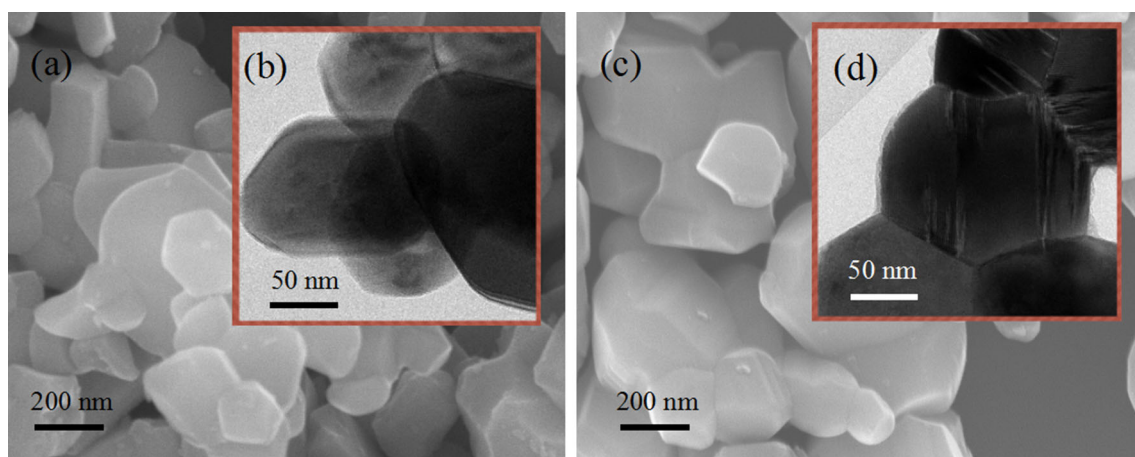


Fig. 1 a SEM and b TEM images of BMCTF without carbon coating, c SEM and d TEM images of C@BMCTF prepared by carbothermal reduction

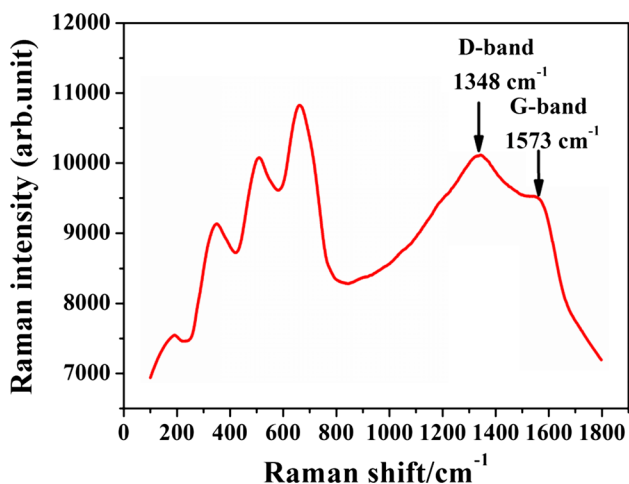


Fig. 2 Raman shifts of sample C@BMCTF

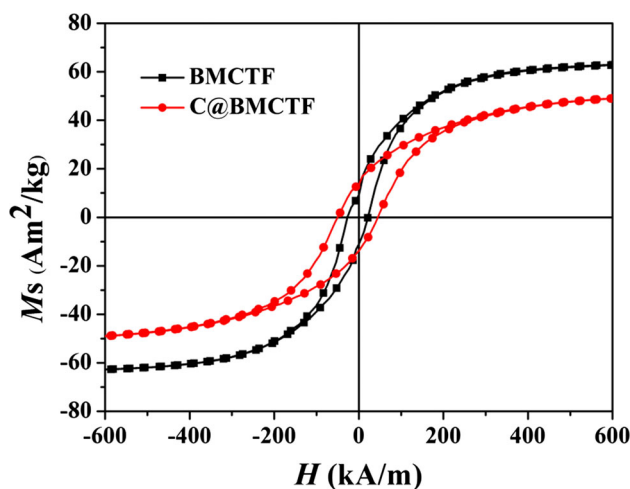


Fig. 4 Magnetic hysteresis loops of BMCTF and C@BMCTF

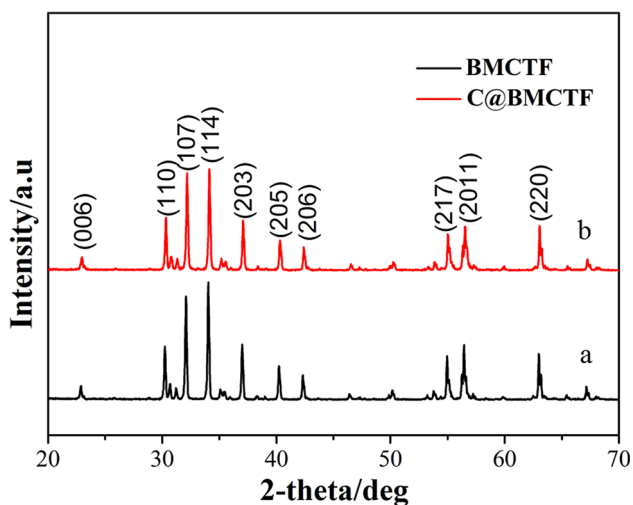


Fig. 3 XRD patterns of (a) BMCTF, (b) BMCTF prepared by carbothermal reduction process (sample C@BMCTF)

BMCTF. Carbon was not visible in the XRD pattern of sample C@BMCTF, because the carbon obtained from glucose under hydrothermal condition was amorphous. However, carbon shell was detected by Raman analysis and was visible in TEM images.

Figure 4 showed the $M-H$ loops of sample BMCTF and C@BMCTF powders. As can be seen in Fig. 4, due to the effect of the carbon coating, C@BMCTF showed less magnetization (M_s) than BMCTF, the reason was that some weight of the coated sample belonging to carbon lacked the magnetization property, and finally led to the decrease of M_s , which were quite perfectly matched with the observed by Jazirehpour et al. [17]. The coercivity (H_c) value of C@BMCTF was greater than that of BMCTF. It was well known that H_c was generally dependent on magnetic phase composition, grain size, structural defects and morphology [22]. Considering the heterojunction layer of C@BMCTF,

the presence of carbon blocked the irreversible displacement of domain wall, and then increased the hysteresis losses of the magnetic nanoparticles, which meant C@BMCTF had a high magneto crystalline anisotropy than that of BMCTF, leading to an increase in H_c . Although the grain size of the ferrite phase was increased slightly after the carbonization process, it just affected the slenderness ratio of the magnetic particles and then indirectly changed the value of coercive force (H_c) [4]. Hence, both the materials were magnetic, and could be used for microwave absorbing applications.

To comprehend the possible microwave absorption mechanism, the real and imaginary part of complex permittivity (ϵ' , ϵ'') and permeability (μ' , μ'') were very important. The real part of relative complex permittivity and permeability were the storing of energy and the imaginary part of relative complex permittivity and permeability were the dissipation of energy [23]. The complex relative permittivity ($\epsilon = \epsilon' - j\epsilon''$) and the complex relative permeability ($\mu = \mu' - j\mu''$) of BMCTF-paraffin and C@BMCTF-paraffin composites were represented in Fig. 5.

Figure 5a and b showed the real part (ϵ') and the imaginary part (ϵ'') of the relative complex permittivity of C@BMCTF and BMCTF, respectively. In Fig. 5a, it was evident that dielectric coefficient of C@BMCTF was increased in comparison to BMCTF. As was known, the permittivity of a material depends upon the extent of various polarizations happening in the material. The possible polarization mechanisms could be classified as ionic, electronic, orientational and space charge polarization [24]. In the microwave range, the active contribution could only be expected from space charge polarization and orientational polarization [17]. The heterogeneity presented in a material was responsible for the space charge polarization

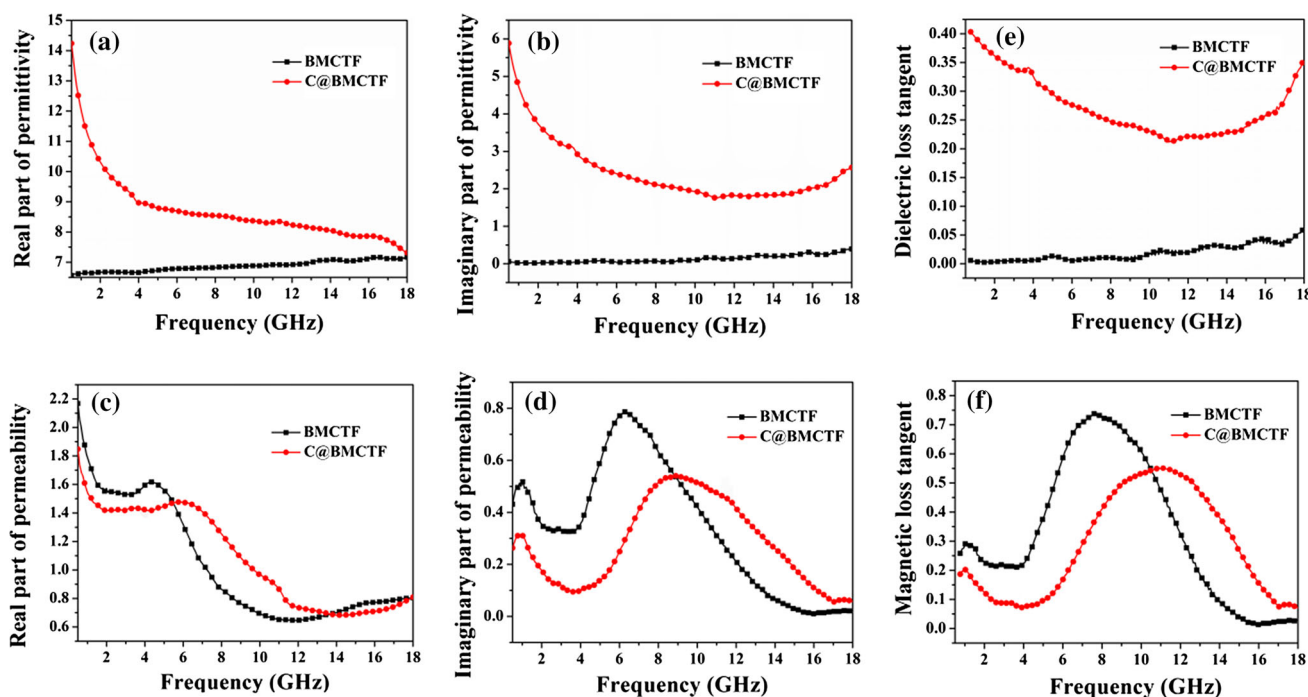


Fig. 5 Variation of dielectric constants of BMCTF and C@BMCTF for different frequencies: **a** real part and **b** imaginary part of complex permittivity, **c** real part and **d** imaginary part of complex permeability, **e** dielectric loss tangent and **f** magnetic loss tangent

and the bound charges presented in a material were responsible for the orientational polarization [25]. In this study, the C shell acted as a dielectric where the orientational polarization could occur effectively [26]. So, the existed of the carbon shell effectively contributed to the dielectric performance of the composite. As shown in Fig. 5b, the value of C@BMCTF of the imaginary part of complex permittivity (ϵ'') drastically augmented in the frequency range of 0.5–18 GHz. To investigate the variation of dielectric loss with the working frequency range, the dielectric loss tangent ($\tan \delta_\epsilon = \epsilon''/\epsilon'$) versus frequency in the range of 0.5–18 GHz was calculated and the image was shown in Fig. 5e. We could find that $\tan \delta_\epsilon$ was significantly improved with the coating of carbon.

As shown in Fig. 5c, we could find that the μ' curve of BMCTF initially declined with the increase of the frequency, which could be related to the limited speed of spin and domain wall movement (displacement/rotation) [27]. Due to the effect of the carbon coating of C@BMCTF, the maximum point of the μ' of C@BMCTF gradually shifted to a higher frequency and the value of the μ' slightly decreased, because the smaller intrinsic saturation magnetization (M_s) value of sample C@BMCTF (Fig. 4) led to smaller μ' coefficient. Observing from the Fig. 5d, it can be seen that the curve of μ'' had a peak and the peak moved to a higher frequency with the coating of carbon. As was known, a higher H_c led to a considerable shift in the resonance frequency to a higher frequency for magnetite

nanoparticles [4, 28]. In this study, the H_c of C@BMCTF (Fig. 4) increased with the coating of carbon, which meant the value of magneto crystalline anisotropy of C@BMCTF was bigger than that of BMCTF. To investigate the variation of magnetic loss with the working frequency range, we also had the relationship of the magnetic loss tangent ($\tan \delta_\mu = \mu''/\mu'$) versus frequency. As shown in Fig. 5f, the value of $\tan \delta_\mu$ changed very little compared with $\tan \delta_\epsilon$, the value of dielectric constant and magnetic permeability had a good match, which meant the HTC carbon coating could be a promising method to increase the dielectric loss and then achieve a better impedance matching of the composites.

The ability of an absorber to absorb the radiation was generally expressed in terms of reflection loss (RL). The greater reflection loss made the better absorbing effect. According to transmission line theory, the reflection loss of EM wave (normal incidence) for a microwave absorbing single layer with a metal back was calculated by the following formula:

$$RL = 20 \log |(Z_{in} - 1)/(Z_{in} + 1)| \quad (1)$$

Z_{in} was given by:

$$Z_{in} = (\mu_r/\epsilon_r)^{1/2} \tanh \left[j(2\pi fd/c)(\mu_r\epsilon_r)^{1/2} \right] \quad (2)$$

where Z_{in} was the normalized input impedance with respect to the impedance in free space and RL was in decibels (dB). ϵ_r ($\epsilon_r = \epsilon' - j\epsilon''$) and μ_r ($\mu_r = \mu' - j\mu''$) were the relative

complex permittivity and permeability of the absorber, c was the velocity of light in free space, f was the frequency and d was the thickness of the absorber [29, 30]. The impedance matching condition was given by $Z_{in} = 1$ to represent the perfect absorbing properties.

Figure 6a showed the RL versus frequency in the range of 0.5–18 GHz for the BMCTF-paraffin composite with different absorbent layer thickness, calculated from Eq. (2). As shown in Fig. 6a, it was noticed that BaMg_{0.2}Co_{0.8}TiFe₁₀O₁₉ composite had a bandwidth below -10 dB (means 90 % absorption) ranging from 5.5 to 11.7 GHz with the thickness of 3.3 mm, and when the thickness of BMCTF composite was 2.9 mm, the maximum RL (-33.5 dB) could be obtained at $f = 11.43$ GHz. The frequency of maximum absorption moved to the lower frequency region with the increase of thickness of the absorber and the range of absorption frequency could be easily tuned by adjusting the thickness of the composite,

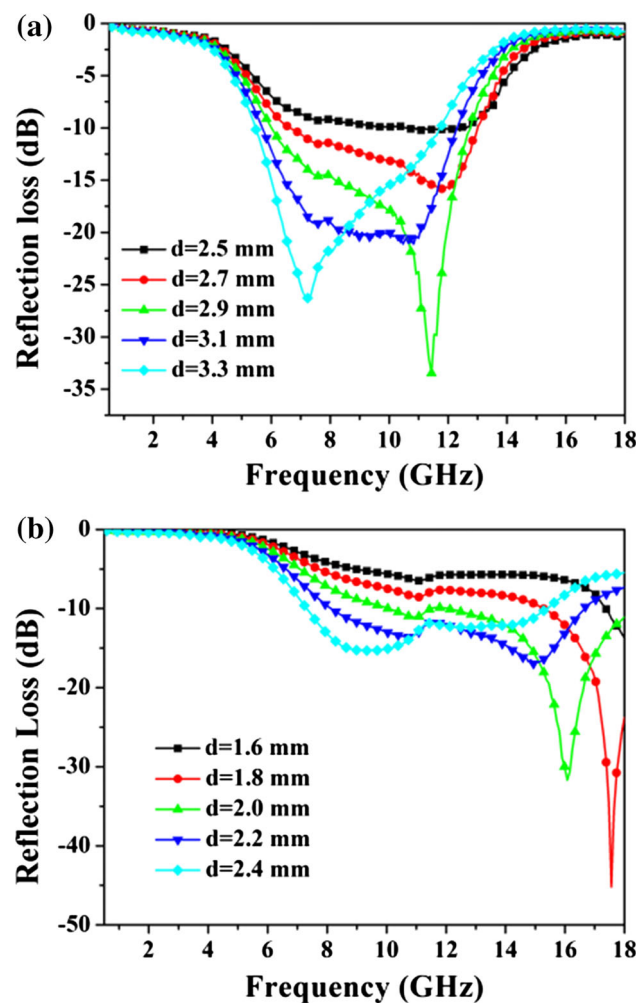


Fig. 6 Reflection loss spectra for BMCTF and C@BMCTF composites: **a** the microwave absorption curves of sample BMCTF with different thicknesses. **b** The microwave absorption curves of sample C@BMCTF with different thicknesses

which were quite perfectly matched with the observation by Bi et al. [31].

The curves of RL versus frequency in the range of 0.5–18 GHz for the C@BMCTF-paraffin composite with different thicknesses were shown in Fig. 6b. It was evident from RL plots that C@BMCTF had a better reflection loss values than BMCTF, which meant C@BMCTF was a better absorbing material. As shown in Fig. 6b, C@BMCTF composite had a bandwidth below -10 dB ranging from 12.14 to 18 GHz with the thickness of 2.0 mm, which can cover the whole Ku band (12.4–18 GHz), and when the thickness of C@BMCTF composite was 1.8 mm, the maximum RL (-45.2 dB) could be obtained at $f = 17.56$ GHz, and when $x = 1.6$ mm, the image suggested that the microwave absorption band would move toward a higher frequency, while the RL could not be confirmed right now because of the limitation of the testing frequency (no more than 18 GHz). Hence, this absorber could be used for different applications according to the requirement by tuning the thickness of the absorber. The BMCTF ferrite has the magnetic loss as the main losses, the value of permeability is much bigger than that of dielectric constant, which led to a narrow band EM absorption. With the addition of carbon, the dielectric constant of the composite increased in the whole GHz, the value of dielectric constant and magnetic permeability have a good match, so electromagnetic wave could enter into the absorber more easily. Hence, the enhanced wave absorption properties of C@BMCTF composite contributed to the increase of dielectric loss. Moreover, the result of the μ'' (Fig. 5d) of C@BMCTF suggested that the microwave absorption band would move toward a higher frequency due to the core-shell structured composite of that magnetic material with C, and the test could be confirmed right now.

4 Conclusions

BMCTF hexaferrites was synthesized by the sol-gel combustion reaction method. The magnetic-dielectric heterostructured nanoparticles (BMCTF as the core and carbon as the shell) were created via a combination of HTC and carbothermal reduction processes. The core-shell structure and morphology were determined by XRD, RAMAN, FE-SEM and HRTEM. Magnetic measurement of C@BMCTF indicated that the H_c could be enlarged with the doping of carbon, whereas the M_s was inversely to the doping. Meanwhile, C@BMCTF exhibited optimum microwave absorption characteristics with a maximum reflection loss (-45.2 dB) when its thickness was 1.8 mm, with the thickness of C@BMCTF composite of 2.0 mm. The bandwidth of RL less than -10 dB was from 12.14 to

18 GHz, which could cover the whole Ku-band. Thus, the composite composed of one dielectric material (C) and magnetic material (BMCTF) with core-shell morphology could be used as a low-cost and high-performance EM absorbing materials.

Acknowledgments This work was supported by Southwest University of Science and Technology (15zx2101).

References

1. X. Jian, X. Chen, Z. Zhou, G. Li, M. Jiang, X. Xu, J. Lu, Q. Li, Y. Wang, J. Gou, *Phys. Chem. Chem. Phys.* **17**, 3024–3031 (2015)
2. L. Wang, Y. Huang, C. Li, J. Chen, X. Sun, *Phys. Chem. Chem. Phys.* **17**, 2228–2234 (2015)
3. S.P. Gairola, V. Verma, V. Pandey, Ravi, L.P. Purohit, R.K. Kotnala, *Int. J.* **119**, 151–156 (2010)
4. J. Chen, P.Y. Meng, M.L. Wang, G.C. Zhou, X.Q. Wang, G.L. Xu, *J. Alloys Compd.* **679**, 335–340 (2016)
5. M. Han, L. Deng, *Appl. Phys. Lett.* **90**, 0111081–0111083 (2007)
6. L. Zhang, C. Shi, K.Y. Rhee, N. Zhao, *Composites A* **43**, 2241–2248 (2012)
7. L. Wang, H.T. Yu, X.H. Ren, G.L. Xu, *J. Alloys Compd.* **588**, 212–216 (2014)
8. P.Y. Meng, K. Xiong, L. Wang, S.N. Li, Y.K. Cheng, G.L. Xu, *J. Alloys Compd.* **628**, 75–80 (2015)
9. X.G. Huang, J. Zhang, L.X. Wang, Q.T. Zhang, *J. Alloys Compd.* **540**, 137–140 (2012)
10. L.B. Kong, Z.W. Li, L. Liu, R. Huang, M. Abshinova, Z.H. Yang, C.B. Tang, P.K. Tang, C.R. Deng, S. Matitsine, *Int. Mater. Rev.* **58**, 203–259 (2013)
11. F.F. Xu, L. Ma, M.Y. Gan, J.H. Tang, Z.T. Li, J.Y. Zheng, J. Zhang, S. Xie, H. Yin, X.Y. Shen, J.L. Hu, F. Zhang, *J. Alloys Compd.* **593**, 24–29 (2014)
12. L.C. Li, K.Y. Chen, H. Liu, G.X. Tong, H.S. Qian, B. Hao, *J. Alloys Compd.* **557**, 11–17 (2013)
13. W.J. Zhang, Y. Bai, X. Han, L. Wang, X.F. Lu, L.J. Qiao, *J. Alloys Compd.* **546**, 234–238 (2013)
14. L. Du, Y.C. Du, Y. Li, J.Y. Wang, C. Wang, X.H. Wang, P. Xu, X.J. Han, *J. Phys. Chem. C* **114**, 19600–19606 (2010)
15. M.K. Tehrani, A. Ghasemi, M. Moradia, R.S. Alam, *J. Alloys Compd.* **509**, 8398–8400 (2011)
16. X.G. Liu, N.D. Wu, C.Y. Cui, Y.T. Li, P.P. Zhou, N.N. Bi, *Mater. Lett.* **149**, 12–14 (2015)
17. M. Jazirehpour, S.A. Seyyed Ebrahimi, *J. Alloys Compd.* **639**, 280–288 (2015)
18. P. Bhattacharya, C.K. Das, *J. Mater. Sci.: Mater. Electron.* **24**, 1927–1936 (2013)
19. L. Ai, J. Jiang, *J. Mater. Sci.: Mater. Electron.* **20**, 257–261 (2009)
20. M.H. Xu, W. Zhong, Z.H. Wang, C. Au, Y.W. Du, *J. Phys. E* **52**, 14–20 (2013)
21. T. Liu, X.B. Xie, Y. Pang, S. Kobayashi, *J. Mater. Chem. C* **4**, 1727–1735 (2016)
22. J.M. Silva, R.S. Nasar, M.C. Nasar, C.L. Firme, J.H. Araujo, *J. Magn. Magn. Mater.* **394**, 274–279 (2015)
23. M. Zong, Y. Huang, N. Zhang, H.W. Wu, *J. Alloys Compd.* **644**, 491–501 (2015)
24. B. Zhao, G. Shao, B.B. Fan, W.Y. Zhao, Y.J. Xie, R. Zhang, *Phys. Chem. Chem. Phys.* **17**, 8802–8810 (2015)
25. Q. Zhang, C. Li, Y. Chen, Z. Han, H. Wang, Z. Wang, D. Geng, W. Liu, Z. Zhang, *Appl. Phys. Lett.* **97**, 13311 (2010)
26. P. Bhattacharya, S. Sahoo, C.K. Das, *Express Polym. Lett.* **7**, 212–223 (2013)
27. R.S. Meena, S. Bhattacharya, R. Chatterjee, *J. Magn. Magn. Mater.* **322**, 2908–2914 (2010)
28. H.L. Xu, Y. Shen, H. Bi, W.F. Liang, R.B. Yang, *Ferroelectrics* **435**, 98–103 (2012)
29. C.S. Dong, X. Wang, P.H. Zhou, T. Liu, J.L. Xie, L.J. Deng, *J. Magn. Magn. Mater.* **354**, 340–344 (2014)
30. Z.T. Zhu, X. Sun, G.X. Li, H.R. Xue, H. Guo, X.L. Fan, X.C. Pan, J.P. He, *J. Magn. Magn. Mater.* **377**, 95–103 (2015)
31. C. Bi, M.F. Zhu, Q.H. Zhang, Y.G. Li, H.Z. Wang, *Mater. Chem. Phys.* **126**, 596–601 (2011)